Chiang Mai J. Sci. 2016; 43(2) : 409-419
http://epg.science.cmu.ac.th/ejournal/
Contributed Paper

Precipitation in the Nugget Zone of AA6061-T6 by Friction Stir Welding

Wang Tao [a], Zou Yong*[a], Kenji Matsuda [b]

[a] Key Lab of Liquid Structure and Heredity of Materials, Ministry of Education, Shandong University, Jinan 250061, Shandong, China.

[b] Department of Materials Science and Technology, Faculty of Engineering, University of Toyama, Toyama, 930-8555, Japan.

*Author for correspondence; e-mail: yzou@sdu.edu.cn

Received: 15 September 2015
Accepted: 13 November 2015

ABSTRACT

Friction stir welding butt welded joints were fabricated successfully for heat-treated AA6061-T6 sheets with 5.85 mm thickness. The influences of welding parameters on structural features, precipitation kinetics and mechanical properties for the obtained welds were investigated by differential scanning calorimetry test, transmission electronic microscopy observation, electron backscattered diffraction and micro-hardness test. Results showed the hardness was influenced by the frequency of low angle gain boundary and precipitation phenomena. The rotation speed mainly has an effect on the frequency of low angle gain boundary, and the feeding speed mainly influences the evolution of precipitates. In addition to β′ and β-Mg_2Si phase in the nugget zone for all the joints, the "u-phase" was found with high feeding speed, and the TYPE-A phase with low feeding speed.

Keywords: Friction stir welding, AA6061-T6, Transmission electronic microscopy, Precipitate

1. INTRODUCTION

The high specific properties of Al alloys due to their low density make them suitable for variety of applications in aerospace and automotive industries. The heat-treated Al-Mg-Si alloy possesses properties like strong, lightweight, high corrosion resistance, high thermal and electrical conductivity, hot and warm formability. There has been a constant effort to improve the strength properties of weld joint of Al in order to meet the ever increasing need of high strength to weight ratio. Friction stir welding (FSW) is an efficient manufacturing method for joining aluminum alloy. As a solid-state process, it has been proved to be very suitable for the plate joint compared to conventional welding methods [1, 2].

It is known that AA6061 contains various strengthening precipitates such as the GP-I zones, GP-II zones (β″), and β′. The specific type, size, and distribution of precipitates have an important impact on mechanical properties. The high density of fine needle shaped β″ precipitate is the main strengthening

source for AA6061-T6. But during FSW process, localized heating is produced between the rotating tool and the work piece, and softens the material below its melting point (typically > 0.5 T_{melt}) [3]. The β″ phase will disappear and evolve to β′ and equilibrium β-Mg_2Si phase during the welding and the hardness values in the NZ (nugget zone) decreased at different degrees depending on different parameters. The post-weld natural aging behavior of FSWed 6005A-T6 Al alloy was investigated by Peng Dong and Daqian Sun [4]. The results show that the original β″ phase disappeared in the NZ due to FSW process. The hardness recovery during post-weld natural aging is attributed to the formation of clusters or GP zones. Dongxiao Li, et al, reported the Stationary shoulder friction stir welding (SSFSW) butt joints of AA6061-T6 sheets and found that the NZ is mainly characterized by small dots which are supposed to be GP-I zones [5]. And the strengthening meta-stable precipitates were all diminished in the nugget zone of the self-reacting friction stir welded butt joints of 6061-T6 Al alloy [6].

The heat input is significant in the FSW of AA6061-T6. The heat input of FSW mainly depends on the ratio between rotation speed and feeding speed. The present work focuses on the application of different welding parameters on friction stir welding of AA 6061-T6 plates, and evaluates the mechanical properties and microstructural characteristics. The type and distribution of the precipitates are mainly analyzed by transmission electron microscopy (TEM) for the nugget zone of the conventional FSW joint. Furthermore, in order to correlate the mechanic property and the microstructural characteristics, the grain structure, dislocation density, precipitation kinetics, etc. were systematically investigated by optical observation, electron backscattered diffraction (EBSD) analysis and differential scanning calorimetry (DSC) test.

2. MATERIALS AND METHODS

2.1 Preparation of The FSW Joints

The AA6061-T6 plates of 5.85 mm thick were cut and machined into rectangular welding samples: 250 mm long and 80 mm wide. The chemical composition is shown in Table 1. Then the plates were butt-welded using an FSW machine (FSW-3LM-3012). The welding tool comprises of a concave shoulder with a diameter of 15 mm and a conical pin with 5.54 mm length and 5 mm diameter at half length. Tool pin is produced with screws left-threaded around the cone to generate the down forging force. The back tilting angle of the tool is 2.5° during FSW. FSW trials were carried out at a feeding speed from 60 to 250 mm/min (millimeter per minute) for various rotation speeds. The welded pieces were cooled in air after welding.

Table 1. Chemical composition of AA 6061-T6 (mass%).

Si	Fe	Cu	Mn	Mg	Cr	Zn	Ti	Ni	Al
0.565	0.340	0.198	0.038	1.005	0.118	0.016	0.024	0.004	Bal.

2.2 Macrograph Observations

The feature of the joint was observed on the transverse cross section. For optical microscopy (OM), the specimens were carefully prepared using the standard metallographic technique consisting of grinding with emery papers up to 2000 grits, followed by diamond polishing to obtain a

mirror-like surface finish, then etched by hydrofluoric acid etchant (HF: 5%, distilled water: 95%).

2.3 EBSD Analysis

For electron backscattered diffraction, specimens were taken through the same procedure for OM and further electro-polished in a solution containing 20vol% perchloric acid and 80vol% methanol at 253 K and 15 V for 30 s to eliminate a plastic-deformed region.

2.4 TEM Investigation

The TEM samples are prepared by Twin Jet Thinning instrument, the work current is 30-50 mA. The foil specimens from the nugget zone were sliced for TEM observation in a Topcon EM-002B transmission electron microscope, using 120 kV or 200 kV operating voltage. The thin sections were subjected to twin-jet electro-polishing in a 100 mL HNO_3 + 400 mL methanol solution at 248 K and 15 V.

2.5 Differential Scanning Calorimetry

To investigate the influence of FSW parameters on precipitated phase, samples cut from the center of the NZ were subjected to DSC analysis using NETZSCH DSC 404C. The polished sample for DSC testing was equilibrated at 30 °C and then heated to 550 °C with a heating rate of 15 °C/min under an argon atmosphere.

2.6 Hardness Test

Vickers hardness was measured at the location of the mid-thickness on the polished transverse cross section using a load of 100 g and dwell time of 15 s with the 0.5 mm distance between successive indentations.

3. RESULTS AND DISCUSSION

3.1 Transverse Section Macrograph of The Joint

The macrographs of transverse section for FSW joints prepared with various tool rotation speeds and various feeding speeds are shown in Figure 1. It is obvious that the defect-free FSW welds were obtained for all the selected welding parameters. The white band pattern is discernable in the NZ from the advancing side to the center, and the geometry of the band pattern varies between different welding parameters. By contrast, the dark and narrow region next to the NZ is the thermal mechanical affected zone (TMAZ). When the feeding speed keeps constant, the band pattern expands in the thickness direction along the interface of NZ and TMAZ with the decreasing of rotation speed. Meanwhile, the band pattern expands to the center of the NZ as the feeding speed increases, when the rotation speed keeps constant. The oxide lazy S is also elongated in transverse direction with the feeding speed decreasing or the rotation speed increasing. This is because the high rotation speed or the low feeding speed produces larger heat input and severe plastic flow.

3.2 TEM Analysis in The Nugget Zone

Figure 2 and Figure 3 show the TEM images and the corresponding SAD patterns of the NZ prepared by using 600 rpm tool rotation speeds and 250 mm/min feeding speeds. The bright field images (Figure 2 (a-b)), indicate that β″ precipitates have disappeared and the rod-shaped precipitates emerged. Basically, the rod-shaped precipitates have two types of cross-sections along [001] Al electron beam direction which are rectangle-shaped and round-shaped.

According to SAD patterns (Figure 2c), the rod-shaped precipitates are identified as the β′ or Q′ phase, since both exhibit very particular features: the {200} spots are nearly extinguished, the intensities of the {100} spots are very weak, the intense spots are the {300} and {210} ones [7]. The corresponding orientation of β′ phase with the Al matrix can be described as: (0001)β′//(001)Al, $[2\bar{1}\bar{1}0]$β′//$[1\bar{3}0]$Al or [310]Al and (approximately) $[\bar{1}2\bar{1}0]$β′//[110]Al or $[\bar{1}10]$Al. The orientation of Q′ phase with the Al matrix can be described as: (0001)Q′//(001)Al, $[2\bar{1}\bar{1}0]$Q′//$[1\bar{5}0]$Al and $[\bar{1}2\bar{1}0]$Q′//[110]Al. Meanwhile, the long-axis of rectangle-shaped precipitates parallels to <310>Al for β′ phase and <150>Al for Q′ phase, respectively [8]. Because the angle between the long-axis of rectangle-shaped precipitates and [100]Al direction is 20°, the rectangle-shaped precipitates are the β′ phase. Besides, the coarse second phase particles in Figure 3(a-b) are β-Mg_2Si. The β phase has two kinds of orientation. One is [001]Al//[001]β and [100]Al//[110]β for conventional cube-shaped phase [9, 10]. The other one is hexagonal tabular β phase discovered in Al-Mg-Si-Cu alloy and its orientation is as follows: [111]Al//[111]β; [110]Al//[110]β [11]. The orientation of β-Mg_2Si phase in the NZ shown in Figure 3c is [001]Al//[001]β and [100]Al//[110]β.

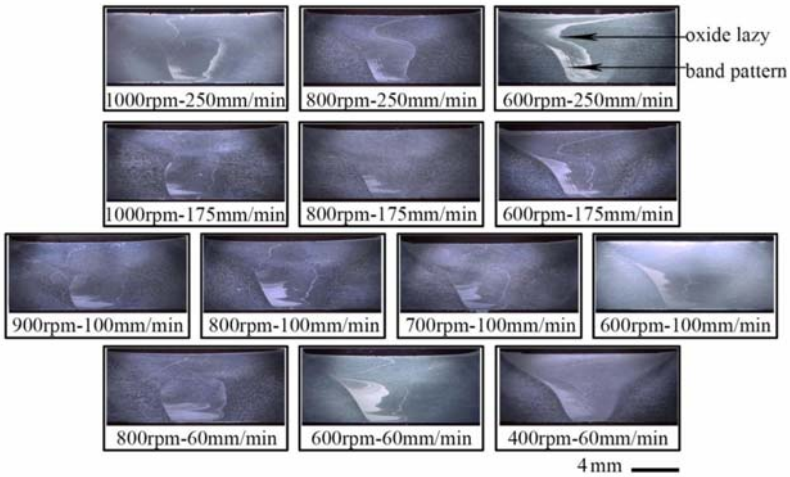

Figure 1. Macrographs of transverse section for FSW joints obtained at various welding parameters.

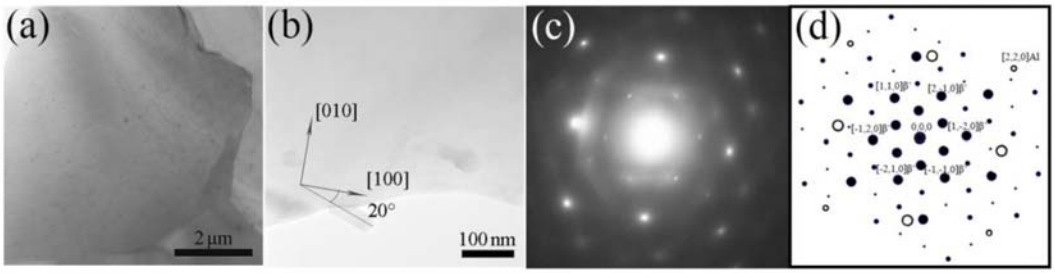

Figure 2. TEM images of the NZ with 600 rpm rotation speed and 250 mm/min feeding speed: (a) and (b) bright field images; (c) electron diffraction patterns from selected zones; (d) simulated SADP of the β′ phase under [0001] zone axis indicated by solid points with the Al matrix indicated by hollow circles.

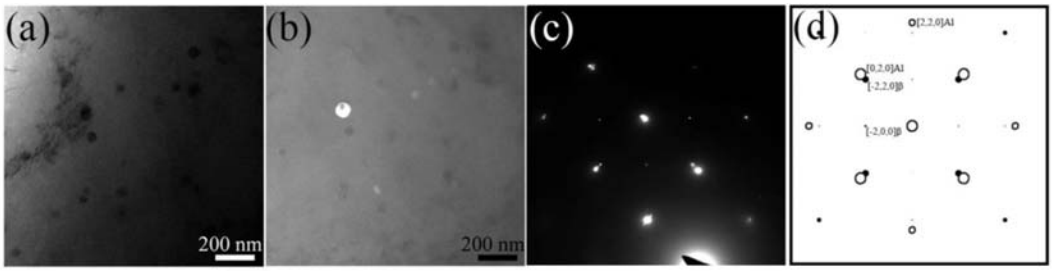

Figure 3. TEM images of the NZ with 600 rpm rotation speed and 250 mm/min feeding speed: (a) bright field image; (b) dark field image; (c) electron diffraction patterns from selected zones; (d) simulated SADP of the β phase under [001] zone axis indicated by solid points with the Al matrix indicated by hollow circles.

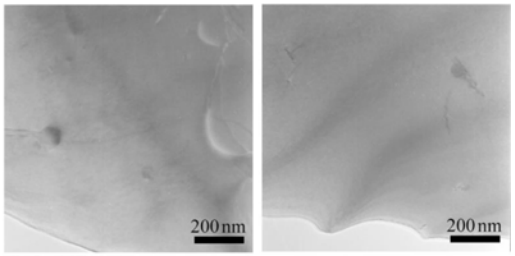

Figure 4. TEM images of the NZ with 800 rpm rotation speed and 175 mm/min feeding speed.

Figure 4 shows another long rod precipitates with a small size formed on the β′ phase in the NZ prepared by using 800 rpm tool rotation speeds and 175 mm/min feeding speeds. It may be the 'u-phase' precipitate which can be nucleated heterogeneously on the dissolving β′ phase when the temperature reaches above ~350 °C [12]. This nucleation event is fairly easy, due to the structural similarity between the β′ and the 'u-phase'. The unit cell of the 'u-phase' is determined to be hexagonal with a=0.670 nm and c=0.808 nm. The c-axis is thus very close to twice the length of the cube length of Al (a_{Al}=4.04 nm). All the composite particles were aligned perfectly in the [100] directions in Al lattice. After a further increase in the temperature, the β′ precipitates will be dissolved completely. Then, α-Al(MnCrFe) Si dispersoids will be heterogeneously nucleated on 'u-phase' containing Mg, Si, Mn, Fe and also probably some Al, and finally consume the 'u-phase' completely into a chain of the dispersoids.

For the NZ welded at low feeding speed, more meta-stable phases are evolve to β-Mg_2Si phase with a high density, as shown in Figure 5 and Figure 6. However, β′ phase is still observed and the corresponding SAD pattern is caused by structure factors and double diffraction under [14$\bar{5}$0]β′// [001]Al zone axis [8, 13]. In addition to β′ phase, the TYPE-A precipitate is also found (Figure 6c), which is in good agreement with calculated result with the incident beam direction [001]TYPE-A//[310]Al [14]. As shown in Figure 6b, it was nucleated on the dislocation. The TYPE-A phase's fundamental lattice is hexagonal with the lattice parameters of a=0.405 nm and c=0.67 nm with the space group of P$\bar{6}$2m. Like TYPE-B and TYPE-C, it usually forms due to the excess Si or a prolonged aging time in the Al-Mg-Si alloys [15]. It is known that different crystallographic orientations often exist within the NZ, and Figure 7 illustrates two inverse pole figure (IPF) maps in welding direction, using the parameters: 600 rpm-250 mm/min; 600 rpm-60 mm/min, respectively. For the NZ welded with

low feeding speed, the materials undergone severe deformation and was elongated with a larger length-width ratio; the different orientations between grain bands is more obvious. Because of heterogeneous plastic deformation within the NZ, the precipitation state is highly related to crystallographic orientations [16]. Thus, the formation of TYPE-A precipitate in the NZ with low feeding speed may be caused by the following reasons: the slower cooling rate; the more obvious difference in orientations between grain bands; last, the released Si atom due to the transformation from β′ to β-Mg_2Si in a larger quantity. The stability of precipitate appears to be closely connected to alloy composition. Then, the alloy tends to select as a precipitate having a Si/Mg ratio closest to the alloy's own Si/Mg ratio [17].

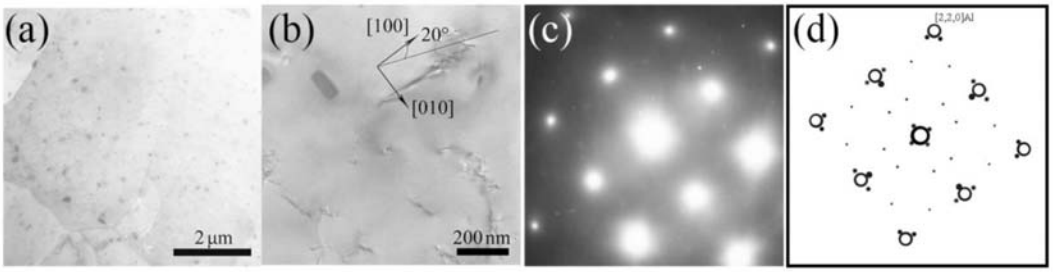

Figure 5. TEM images of the NZ with 400 rpm rotation speed and 60 mm/min feeding speed: (a) and (b) bright field images; (c) electron diffraction patterns from selected zones; (d) simulated SADP of the β′ phase under [14$\bar{5}$0] zone axis indicated by solid points with the Al matrix indicated by hollow circles.

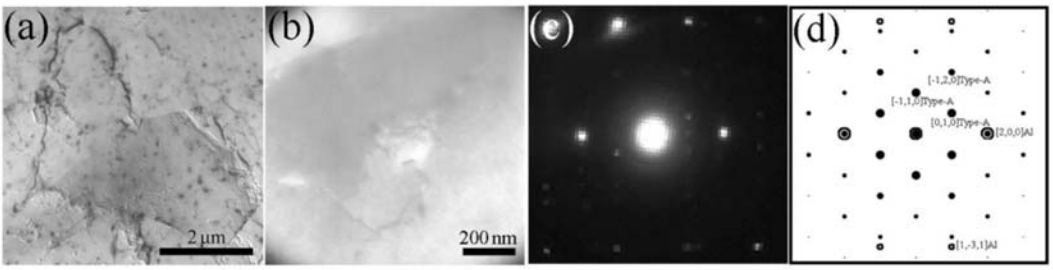

Figure 6. TEM images of the NZ with 600 rpm rotation speed and 60 mm/min feeding speed: (a) and (b) bright field images; (c) electron diffraction patterns from selected zones; (d) simulated SADP of the TYPE-A phase under [001] zone axis indicated by solid points with the Al matrix indicated by hollow circles.

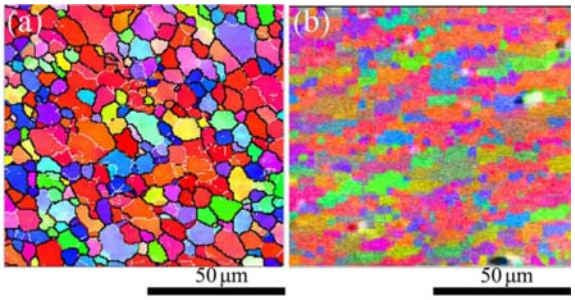

Figure 7. IPF maps of the NZ obtained by EBSD analysis with various parameters: (a) 600 rpm - 250 mm/min; (b) 600 rpm - 60 mm/min.

3.3 Hardness of The Joint

The transverse micro-hardness distribution on the cross-sections of the joints is shown in Figure 8 and Figure 9. The micro-hardness distribution profiles exhibit W-shape and are corresponding to four distinct microstructural zones, namely, NZ, TMAZ, HAZ and BM. The micro-hardness in the welded zone is strongly reduced in contrast to the BM, and the micro-hardness profile is asymmetry on the advancing side and the retreating side of the FSW joint. It can be seen that the micro-hardness of the BM is about 110 HV and the softest region locates in HAZ adjacent to the TMAZ. In most cases, the width of NZ and HAZ increases with the increasing of rotation speed and the decreasing of feeding speed. When feeding speeds of 60 and 100 mm/min are employed, the NZ hardness is higher at high tool rotation speeds than at low tool rotation speeds. However, for the joints made using 175 and 250 mm/min feeding speeds, there is an unconspicuous downtrend in the hardness of NZ as the rotation speed increases. Furthermore, the NZ hardness is higher at high feeding speeds than at low feeding speeds when a constant rotation speed is given.

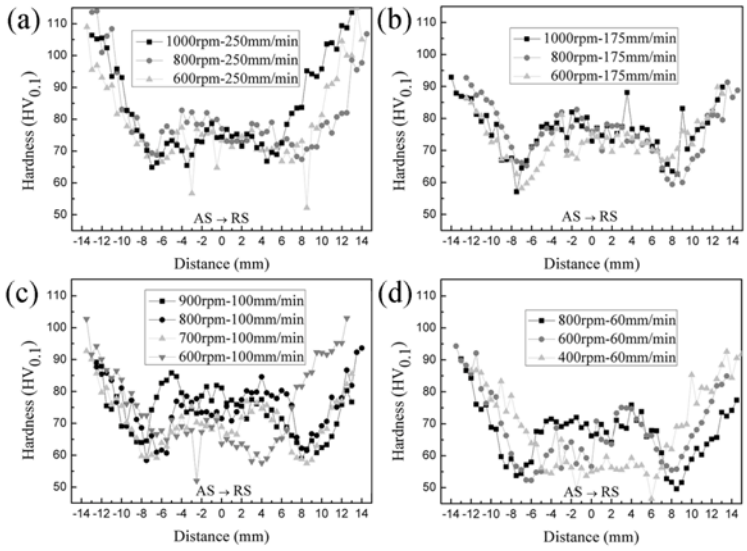

Figure 8. Hardness profile on the mid-thickness line of FSW joints made using various feeding speeds: (a) 250 mm/min; (b) 175 mm/min; (c) 100 mm/min; (d) 60 mm/min.

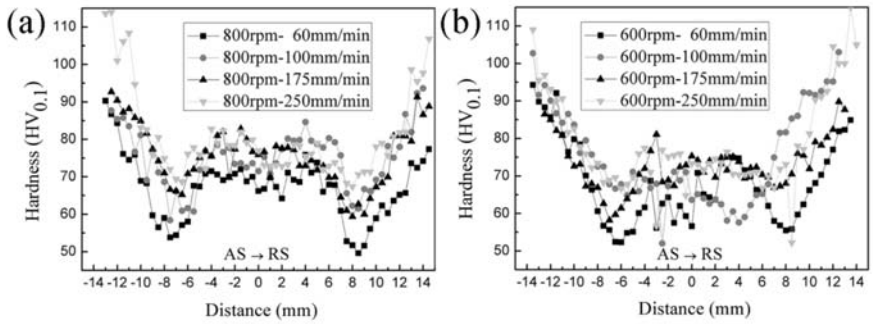

Figure 9. Hardness profile on the mid-thickness line of FSW joints made using various rotation speeds: (a) 800 rpm; (b) 600 rpm.

3.4 Precipitation Kinetics

The main aim of the DSC analysis is to evaluate the precipitation kinetics in the NZ of AA6061-T6 by FSW. Samples prepared at different FSW parameters were analyzed by DSC equipment as shown in Figure 10 and Figure 11. Usually, the formation of solute-rich clusters occurs at 50-80 °C. And the formation of Si-Mg-vacancy clusters occurs at 120~140 °C. The exothermic reaction peaks of β″, β′ and β, are observed at temperature of 180~250 °C, 250~320 °C and 380~470 °C, respectively. Between the exothermic peaks of β′ and β, there may exist some other meta-stable phases, such as TYPE-A, TYPE-B, TYPE-C or the "u-phase".

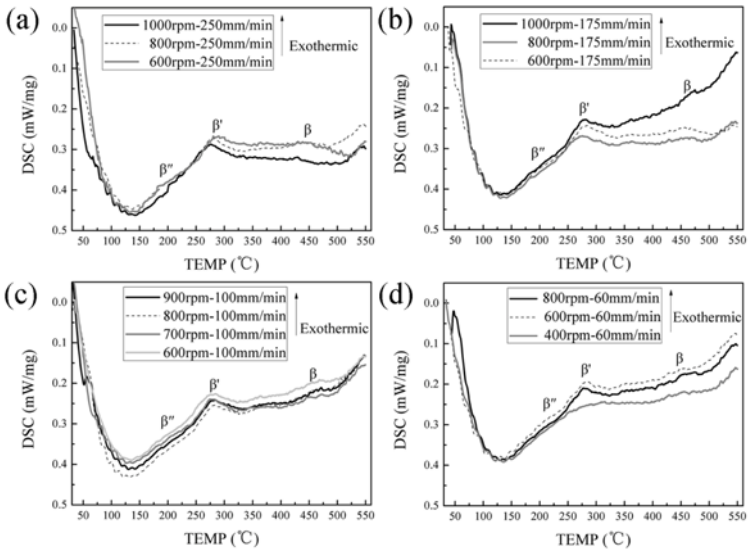

Figure 10. DSC plots for heat flow of precipitate reactions of the center region in the NZ, feeding speeds: (a) 250 mm/min; (b) 175 mm/min; (c) 100 mm/min; (d) 60 mm/min.

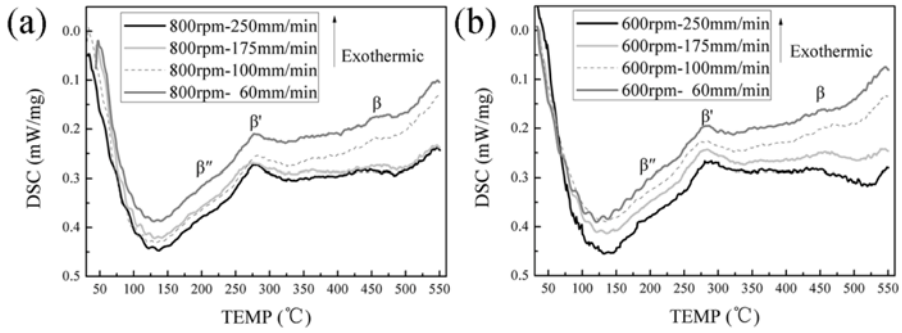

Figure 11. DSC plots for heat flow of precipitate reactions of the center region in the NZ, rotation speeds: (a) 800 rpm; (b) 600 rpm.

Normally, the dislocation density, grain size and precipitation phenomena will influence the hardness. Recent research reveals that: the precipitation plays a dominant role in stored energy in the NZ, while the contribution of the low grain boundary and dislocation is negligible in DSC analysis [18]. Due to similar DSC curves below 250 °C among different rotation speeds at a constant feeding speed (Figure 10(a-b)) and

the distinctive frequency of low angle gain boundaries (Figure 12(a-b)), it indicates the similar hardness of the NZ using high feeding speeds (250 mm/min and 175 mm/min) (Figure 8(a-b)) results from the increased frequency of low grain boundary and more transformation from meta-stable phases to Mg_2Si as the rotation speed increases. The high frequency of low grain boundary will increase the hardness, but the reduced meta-stable precipitate will decrease the hardness in the contrary. The formation of "u-phase" and α-Al(MnCrFe)Si dispersoids will consume many atoms like Si, Mn, Cr and Fe, which have a smaller diameter than Al atom. Besides, the atomic ratio of β-Mg_2Si phase is similar to that of β′-Mg_9Si_5 when the alloy is over-aged. The evolution of the precipitates containing Mg and Si and the formation of dispersoids containing Mn and/or Cr occur independently, and dispersoids containing Mn and/or Cr form during continuous heating above 400 °C. So the formation of "u-phase" and dispersoids can lead lattice constants of the matrix to increase, and the diffraction angles decrease with the increasing of rotation speed, as shown in Table 2.

However, the hardness in the NZ is distinctive between high tool rotation speeds and low tool rotation speeds when the feeding speeds are lower (100 mm/min and 60 mm/min) (Figure 8(c and d)). There also exists a similarity in the DSC curves below 250 °C (Figure 10(c and d)). The reason may be explained that the meta-stable phases have transformed to balance Mg_2Si phase with a great extent. Therefore, the hardness is mainly influenced by the high frequency of low grain boundary induced by high rotation speed. So, the diffraction angles remain nearly the same regardless of the rotation speed at low feeding speed.

Table 2. XRD data of longitudinal cross section of the center of the NZ.

	2-Theta (°)		
Parameters	(111)	(002)	(022)
1000rpm-250mm/min	38.28	44.519	64.878
800rpm-250mm/min	38.341	44.595	64.941
600rpm-250mm/min	38.38	44.638	64.963
1000rpm-175mm/min	38.322	44.561	64.92
800rpm-175mm/min	38.363	44.601	64.959
600rpm-175mm/min	38.376	44.603	64.943
900rpm-100mm/min	38.323	44.56	64.918
800rpm-100mm/min	38.32	44.561	64.92
700rpm-100mm/min	38.339	44.564	64.938
600rpm-100mm/min	38.319	44.56	64.918
800rpm-60mm/min	38.304	44.557	64.902
600rpm-60mm/min	38.38	44.602	64.977
400rpm-60mm/min	38.303	44.541	64.899

It should be noted that unlike the GP zones in the binary Al-Cu alloys, which produce streaks along the <100> direction, GP-I zones in Al-Mg-Si alloys do not produce any streaks. It is difficult to detect the GP-I zones from SADP [4]. As it is discussed above, the distinctive DSC curves below 250 °C between different feeding speeds at a constant rotation speed and the similar frequency of low angle gain boundaries (Figure 12(b and c)) indicate the re-precipitation of more GP zones or a larger residual stress the NZ with the decreasing of feeding speed. Nevertheless, the NZ hardness is higher at high feeding speeds than at low feeding speeds when keeping a constant rotation speed. Thus, the less depletion of meta-stable phases (β″ and β′), and the larger residual stress maybe, rather than the re-precipitation of GP zones, has a more obvious effect on the hardness of the NZ. Besides, refer to the exothermic peaks of the DSC curves above 250 °C, the formation of β-Mg_2Si phase is found outstanding at low feeding speed. It's

possible that, as the feeding speed decreased, some meta-stable β′ transformed to more stable precipitates like TYPE-A, which are prepared to turn into β-Mg_2Si when heated during the DSC testing.

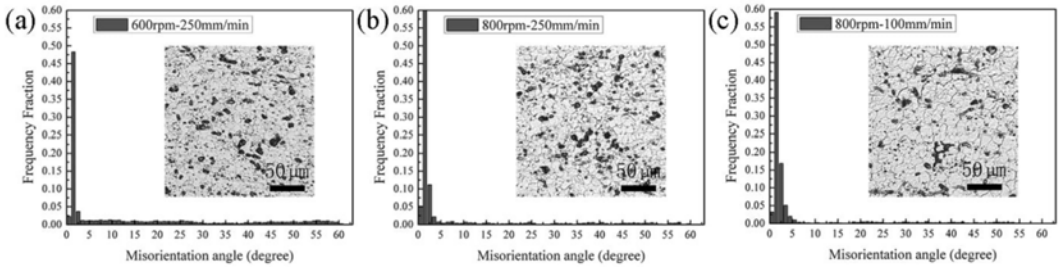

Figure 12. Histograms illustrating the distribution of the misorientation in the center of the NZ: (a) 600 rpm - 250 mm/min; (b) 800 rpm - 250 mm/min; (c) 800 rpm - 100 mm/min.

4. CONCLUSIONS

(1)The high rotation speed and low feeding speed can affect the precipitate of the nugget zone of AA6061-T6 FSW joint due to producing larger heat input and severe plastic flow. The β′ and β-Mg_2Si phases were observed in the nugget zone. Furthermore, the "u-phase" was also found in the NZ by high feeding speeds, and the TYPE-A precipitate by low feeding speed.

(2)The rotation speed also has an effect on frequency fraction of the low grain boundary. The hardness of the NZ is higher at high tool rotation speed than low tool rotation speed at the feeding speed of 60 and 100 mm/min. There is an unconspicuous downtrend in the hardness of NZ by increasing the rotation speed at the feeding speeds of 175 and 250 mm/min. The difference may be explained as the evolution of meta-stable phases (β″ and β′) to a great extent when the feeding speed is lower, which will not influence the hardness obviously with the increasing of rotation speed, compared to the frequency of low grain boundary.

(3)The hardness of NZ is higher at high feeding speeds than at low feeding speeds when a constant rotation speed is given. It is mainly caused by the more disappearance of meta-stable phases (β″ and β′) due to lower feeding speed, even though the re-precipitation of more GP zones may occur at the same time.

ACKNOWLEDGEMENT

This research is supported financially by National Natural Science Foundation of China (NO.51271099). The authors are grateful to J.M. Zuo and J.C. Mabon for TEM analysis by using the Web-based Electron Microscopy Application Software: Web-EMAPS, available from: http://emaps.mrl.uiuc.edu/default.asp.

REFERENCES

[1] Mishra R.S. and Ma Z.Y., *Mat. Sci. Eng. R.*, 2005; **50**: 1-78.

[2] Nandan R., DebRoy T. and Bhadeshia H., *Prog. Mater. Sci.*, 2008; **53**: 980-1023.

[3] Chang C.I., Du X.H. and Huang J.C., *Scripta Mater.*, 2007; **57**: 209-212.

[4] Dong P., Sun D.Q. and Li H.M., *Mat. Sci. Eng. A-struct*, 2013; **576**: 29-35.

[5] Li D.X., Yang X.Q., Cui L., He F.Z. and Shen H., *Mater. Design.*, 2014; **64**: 251-260.

[6] Liu H.J., Hou J.C. and Guo H., *Mater. Design.*, 2013; **50**: 872-878.

[7] Cayron C. and Buffat P.A., *Acta Mater.*, 2000; **48**: 2639-2653.

[8] Yang W., Wang M., Sheng X., Zhang Q. and Huang L., *Phil. Mag. Lett.*, 2011; **91**: 150-160.

[9] Matsuda K., Ishida Y., Mullerova I., Frank L. and Ikeno S., *J. Mater. Sci.*, 2006; **41**: 2605-2610.

[10] Matsuda K., Kawabata T., Uetani Y., Sato T. and Ikeno S., *J. Mater. Sci.*, 2002; **37**: 3369-3375.

[11] Matsuda K., Kawabata T., Uetani Y., Sato T. and Ikeno S., *Scripta Mater.*, 2002; **47**: 467-471.

[12] Lodgaard L. and Ryum N., *Mat. Sci. Eng. A-struct*, 2000; **283**: 144-152.

[13] Vissers R., van Huis M.A., Jansen J., Zandbergen H.W., Marioara C.D. and Andersen S.J., *Acta Mater.*, 2007; **55**: 3815-3823.

[14] Matsuda K., Tada S., Ikeno S., Sato T. and Kamio A., *Scripta Metal. Mater.*, 1995; **32**: 1175-1180.

[15] Matsuda K., Sakaguchi Y., Miyata Y., Uetani Y., Sato T., Kamio A. and Ikeno S., *J. Mater. Sci.*, 2000; **35**: 179-189.

[16] Proton V., Alexis J., Andrieu E., Delfosse J., Lafont M.C. and Blanc C., *Corros. Sci.*, 2013; **73**: 130-142.

[17] Marioara C.D., Nordmark H., Andersen S.J. and Holmestad R., *J. Mater. Sci.*, 2006; **41**: 471-478.

[18] Dai Q.L., Liang Z.F., Wu J.J., Meng L.C. and Shi Q.Y., *Acta Metall. Sin.*, 2014; **50**: 587-593.